# Study on k-ω-Shear Stress Transport Corrections Applied to Airfoil Leading-Edge Roughness Under RANS Framework

Gutiérrez, R.; Llorente, E.; Ragni, D.; Aranguren, P.

**DOI**
10.1115/1.4052925

**Publication date**
2022

**Document Version**
Final published version

**Published in**
Journal of Fluids Engineering, Transactions of the ASME

**R. Gutiérrez**
Nordex Energy Spain S.A.U.,
Sarriguren,
Navarra 31621, Spain
e-mail: RGutierrez@nordex-online.com

**E. Llorente**
Nordex Energy Spain S.A.U.,
Sarriguren,
Navarra 31621, Spain
e-mail: ELlorente@nordex-online.com

**D. Ragni**
Aerodynamics, Wind-Energy and Flight
Performance and Propulsion AWEP Department,
Delft University of Technology
HS 2629 Delft, The Netherlands
e-mail: D.Ragni@tudelft.nl

**P. Aranguren**
Department of Engineering,
Public University of Navarre,
Pamplona, Navarra 31006, Spain
e-mail: patricia.arangureng@unavarra.es

# Study on $k-\omega-$Shear Stress Transport Corrections Applied to Airfoil Leading-Edge Roughness Under RANS Framework

*A computational fluid dynamics study is carried out to model the effects of distributed roughness at the airfoil leading-edge using the equivalent sand grain approach and Reynolds-averaged Navier–Stokes equations. The turbulence model $k-\omega-$shear stress transport (SST) is selected to emulate a fully turbulent flow. Three k and ω boundary conditions are studied to model roughness effects. One refers to Wilcox's boundary condition and the other two refer to Aupoix's boundary conditions. Besides, Hellsten's correction is used to ensure Wilcox's boundary condition compatibility with the shear stress transport limiter. After validating the implementation of these boundary conditions, they are applied to three different airfoils. One of them is a thick airfoil with industrial relevance. For this airfoil, Wilcox's boundary condition significantly underestimates the roughness impact on aerodynamic coefficients. The pressure gradient simplification in Wilcox's boundary condition formulation is the driving factor behind this effect. The pressure gradient effect on Aupoix's boundary condition is minimal.*
[DOI: 10.1115/1.4052925]

## 1 Introduction

Modern computations of turbulent flows over aerodynamically shaped bodies, like wind turbine blades, involve the solution of the Navier–Stokes equations (N–S equations) along with a closure module of the turbulence when this cannot be directly computed [1]. Wind turbine blades are typically discretized into blade sections to lower the computational costs [2]. Even though the modeling fidelity of turbulence has been increased by large eddy simulation and detached eddy simulation approaches [3], Reynolds-averaged Navier–Stokes (RANS) is the most selected approach due to its affordability. In airfoil applications, eddy viscosity models are mostly chosen under the RANS framework to model a fully turbulent state. Spalart and Allmaras [4] and $k-\omega-$shear stress transport (SST) [5] models are the most used in airfoil applications. To model the flow at the transition location, more equations are added to the turbulence closure problem. Some examples are the transitional models $\gamma-\mathrm{Re}-\theta$ [6] and $k-\mathrm{kl}-\omega$ [7].

For these computations, the surface state of wind turbine blades is usually modeled assuming a smooth surface. Roughness elements, if present, are treated as embedded elements inside the viscous sublayer of the boundary layer (BL).

Nevertheless, efforts are taken in the wind energy sector to predict the impact on wind turbines' performance caused by surface roughness. The worsening of the aerodynamic blade response implies a loss of annual energy production (AEP) [8]. The surface roughness impact has been reduced by the use of blade pitch control going from 25% of AEP loss in stall regulation [9] to 5% in pitch regulation. However, a wide range of AEP loss can be found in the literature. The sensitivity of the empirical [10] and computational methods [8] justifies the difference in AEP estimation.

High-lift airfoils are typically used in modern wind turbines, which are characterized by a pressure coefficient distribution built up close to the leading edge. A rough surface at this specific location might alter the properties of the pressure gradient resulting in decreased airfoil performance. This is likely to occur because this region is the most subjected one to erosion during wind turbine operation.

Four main effects are produced by roughness on airfoil performance:

(1) Velocity shift in logarithmic BL region: Nikuradse's experiments [11] revealed a displacement of the logarithmic region of the BL, $\Delta u^+$, caused by sand grains attached to the walls of a pipe.
(2) Turbulence intensity (TI) increase: the interaction of the roughness elements when the BL modifies the turbulent profile [12].
(3) Anticipation of transition location [13].
(4) Induced separated flow: Roughness elements strongly perturb the BL by decreasing the flow momentum needed to overcome the adverse pressure gradient (APG). As a result, flow separation occurs downstream of the roughness elements. Gutiérrez et al. [10] measured this flow separation on the pressure side of a 30% thick airfoil.

The combination of these four effects results in losses of maximum lift coefficient $C_{\mathrm{Lmax}}$ and lift coefficient $C_{\mathrm{L}}$ slope, as well as an increment in drag coefficient $C_{\mathrm{D}}$.

Panel methods, like the ones implemented in XFOIL [14] or RFOIL [15] softwares, are used to compute the airfoil aerodynamic coefficients. These software model the turbulent transition using the $e^N$ method [16]. The turbulence growth caused by roughness can be adjusted with the $N$ factor, whereas the transition anticipation can be specified at a precise stream-wise location. In finite volume methods, the fully-turbulent $k-\omega-$SST model is typically used to emulate the BL development on the surface of rough airfoils [17].

Aupoix [18] classified a group of modeling methods based on the order of approximation of the roughness distribution geometry. The mesh resolution needed to correctly discretize the roughness elements makes the selection of high-order methods unaffordable. A few studies purely focused on academic applications [19], can be found in the literature. On the other hand, low-order methods do not account for the details of the roughness; but instead, they modify the set of equations to indirectly introduce the roughness effects on the flow.

Among the variety of low-order methods, Aupoix [18] recommended the discrete element method (DEM) and the equivalent

Contributed by the Fluids Engineering Division of ASME for publication in the JOURNAL OF FLUIDS ENGINEERING. Manuscript received March 12, 2021; final manuscript received October 29, 2021; published online February 7, 2022. Editor: Francine Battaglia.

  

sand grain approach. The DEM modifies the N–S equations to introduce the flow blockage caused by roughness elements. The equivalent sand grain approach enhances the eddy viscosity near the wall via the use of specific boundary conditions (BCs). A modified value of turbulence quantities is established at the wall. As a result, the velocity profile is displaced and the friction increases. Thus, the implementation of these boundary conditions is more affordable than DEM modifications.

Hence, airfoil flows subjected to roughness have mainly been studied using the equivalent sand grain method. Despite some models assume the transition anticipation on rough surfaces [13], studies based on the fully turbulent BL development with the $k-\omega-$SST model are the most common ones. Aupoix [20] checked the compatibility of the current roughness corrections with $k-\omega-$SST using flat plate cases. The solution of a simplified set of sublayer equations revealed an underestimation of the velocity displacement ($\Delta u^+$) once Wilcox's BC was used along with Hellsten's correction. To solve the weaknesses of the BCs compatibility, Aupoix suggested two novel BCs to improve the $\Delta u^+$ prediction for a wide range of roughness flow conditions. The quantification of this improvement in terms of airfoil performance is the aim of this study. For this purpose, a thicker airfoil than the ones found in the literature [21] is chosen. As a result, roughness corrections are studied along with RANS limitations to predict flow separation in thick airfoils [22].

The equivalent sand grain approach is used in this study. Three different BCs are implemented in the open-source computational fluid dynamics (CFD) solver OPENFOAM [23]. The Wilcox's BC along with Hellsten's correction is selected to validate the most common BC in the airfoil cases found in the literature. Aupoix's BCs are also used to verify a possible improvement on the prediction of the airfoil aerodynamic coefficients. This study aims to find out the limits of these methods once they are applied to thick airfoils. The theoretical background of each method is described in Sec. 2. The numerical modeling setup is described in Sec. 3. A flat plate case is used to validate the methodology in Sec. 4. The computational validation follows in Sec. 5 with airfoil cases taken from literature. After BCs validation, a novel airfoil test case is studied in Sec. 6. Finally, conclusions are drawn in Sec. 7.

## 2 Theoretical Background

The equivalent sand grain approach inherits its name from the concept defined by Schlichting and Gersten [24]. Nikuradse [11] studied the roughness effects on the overlap region of the BL. An array of sand grains with a precise height was used in his experiments to emulate a rough surface. Later, Schlichting defined the equivalent sand grain roughness $k_s$ as the roughness height, which in Nikuradse's experiments, would provide the same friction increment as a technical roughness $k_{tech}$ does in the fully rough regime. Hence, the friction of the technical roughness can be quantified using the Nikuradse's law (see Eq. (4)). Figure 1 shows a schematic equivalence of the Schlichting's concept.

Roughness elements act on different regions inside the BL. These regions are bounded by $y^+$ ranges. According to Eq. (1), the shear stress at the wall $\tau_w$ is required to compute the friction velocity $u_\tau$ and to transfer the physical wall normal distance $y$ to the flow magnitude $y^+$. The viscous sublayer of the BL is defined for $y^+$ values below 30 where the relationship $u^+ = y^+$ holds. The logarithmic layer follows Eq. (2) and is defined for $y^+$ values higher than 70. A value of 5 is usually assigned to the empirical constant $C^+$ [24] used in Eq. (2). The buffer layer is defined for intermediate $y^+$ values

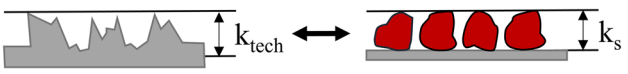


**Fig. 1 Representation of the equivalence between $k_{tech}$ and $k_s$ concepts**

$$u^+ = \frac{u}{u_\tau} \quad y^+ = \frac{y \cdot u_\tau}{\nu} \quad u_\tau = \sqrt{\frac{\tau_w}{\rho}} \tag{1}$$

$$u^+ = \frac{1}{\kappa}\ln y^+ + C^+ \tag{2}$$

Similarly to the definition of $y^+$, $k_s$ is related to flow conditions through the parameter $k_s^+$

$$k_s^+ = \frac{k_s \cdot u_\tau}{\nu} \tag{3}$$

Nikuradse transformed Eq. (2) in Eq. (4) to introduce the $\Delta u^+$ produced by roughness

$$u^+ = \frac{1}{\kappa}\ln\frac{y^+}{k_s^+} + B\left(k_s^+\right) \tag{4}$$

The function $B(k_s^+)$ depends on $k_s^+$ and introduces the $\Delta u^+$ shift for different flow conditions. Nikuradse defined three different regimes of $k_s^+$:

$k_s^+ < 5$ the surface can be considered smooth.

$k_s^+ > 70$ a fully rough regime is assumed. Only the pressure imbalance across the roughness elements contributes to drag.

$5 < k_s^+ < 70$ the intermediate regime is called transitional regime in which friction forces also contribute to drag. Colebrook et al. [25] and Colebrook [26] carried out several experiments to verify the non-universal character of the transition regime.

Nikuradse used the values $\kappa = 0.4$ and $C^+ = 5.5$ in Eq. (4) while values of $\kappa = 0.41$ and $C^+ = 5$ are used in Eq. (2). These last values are more consistent with the calibration of the $k-\omega-$SST turbulence model. To cope with this discrepancy, Aupoix recommended to use Gridgson's [27] representation of the Colebrook's experiments (Eq. (5) where $\kappa = 0.41$ and $C^+ = 5.25$). The term $\exp[\kappa(8.5 - C^+)]$ in Eq. (5), is the intercept of the fully rough asymptote in the roughness function $\Delta u^+(k_s^+)$, where the value 8.5 refers to the value $B(k_s^+)$ given by Nikuradse for the fully rough regime ($k_s^+ > 70$)

$$\Delta u^+ = \frac{1}{\kappa}\ln\left(1 + \frac{k_s^+}{\exp[\kappa(8.5 - C^+)]}\right) \tag{5}$$

Equations (3), (4), and (5) are extensively used throughout this study as these equations are intrinsically included in the mathematical expressions of the boundary conditions used in Secs. 4, 5, and 6.

Historically two paths have been followed, either turbulence models have been improved or boundary conditions have been developed to model roughness effects. Menter stated the new baseline $k-\omega$ model (BSL) to improve the dependency of the Standard $k-\omega$ of Wilcox to freestream values. Later, Menter added the SST limiter to the BSL to improve the performance under APG which are considered crucial for airfoil computations. However, some incompatibilities have been found between the BCs and the SST limiter.

Part of the explanation given by Aupoix [20] is used along the Secs. 2.1–2.3. This study intends to find out the limits of this theory when applied to airfoil cases.

**2.1 Wilcox's Boundary Condition.** The turbulence model standard $k-\omega$ developed by Wilcox allows the specification of arbitrary values of $\omega$ at the wall. This feature was originally discovered by Saffman and Whitham [28] and was taken by Wilcox [3] to create a $\omega$ boundary condition to be set at rough walls. A function $S_R$ was fitted to Nikuradse data to match the same velocity shift. This fitting was carried out using a time marching

procedure to solve a simplified set of sublayer equations. The convective term and the pressure gradient term were neglected in those equations

$$\omega_w = \frac{u_\tau^2 S_R}{\nu} \qquad S_R = \begin{cases} \left(\frac{50}{k_s^+}\right)^2 & k_s^+ \le 25 \\ \frac{100}{k_s^+} & 25 < k_s^+ < 2000 \end{cases} \tag{6}$$

Near a smooth wall, small eddies are expected with a $\omega$ value that tends to infinity. As remarked by Aupoix [20], a finite specific dissipation is now imposed by the BC at the wall, which will lead to turbulence enhancement. Consequently, a relatively higher momentum transfer toward the wall is reported in the literature.

**2.2 Hellsten's Correction to Wilcox's Boundary Condition.** Menter's $k-\omega$ turbulence models preserve part of the original Standard $k-\omega$ formulation for a BL height below half of the BL thickness $\delta$. While Wilcox's BC behaves adequately for the BSL model, Hellsten and Laine [29] demonstrated its incompatibility for $k-\omega-$SST. Above a fully rough surface, the SST limitation becomes active in the roughness layer. Menter designed the SST limiter to introduce the Bradshaw's assumption at the outer region of the BL, which is not valid for the inner region of the BL. Consequently, an underestimation of the roughness effect occurs.

Hellsten and Laine [29] used the ratio $(F_2|\mathbf{S}|/(a_1\omega))$ to assess the activation of the SST limiter. If this ratio exceeds 1, the SST limiter is enabled. The specification of a finite value of $\omega$ at the wall increases the value of the ratio because the term $a_1\omega$ is smaller than the $\infty$ value of the one used for smooth walls. The $F_2$ function, introduced in Eq. (7), was designed by Menter to deactivate the SST limiter in regions of free-shear flows. Similarly, a $F_3$ function was added to the $\mu_t$ definition by Hellsten and Laine [29] to prevent the activation of the SST limiter in the viscous-sublayer. $F_3$ function is set to zero in the near-wall region and is one elsewhere

$$\mu_t = \frac{a_1 \rho k}{\max(a_1\omega; b_1|\mathbf{S}|F_2F_3)} \tag{7}$$

As implemented in OPENFOAM 5.0

$$F_3 = 1 - \tanh\left[\min\left(\frac{150\nu}{\omega y^2}; 10\right)^4\right] \tag{8}$$

The $F_3$ function is already implemented in the source code as a switch option. So, only the implementation of the Wilcox's BC was necessary for this part of the study.

**2.3 Aupoix Boundary Conditions.** Aupoix demonstrated that Wilcox's BC along with Hellsten's correction underestimates the velocity shift for large roughness ($k_s^+ > 1000$). Aupoix justified this failure with the difference in the diffusion coefficient $\sigma_k$ between BSL and SST models.

Aupoix [20] stated that all previous BCs could not provide with suitable prediction for the entire roughness regime. Consequently, two new sets of BCs were developed concerning a simplification of the Aupoix's general method to extend turbulence models to rough surfaces [18]. Given a reduced roughness height $k_s^+$, the solution of the model over a smooth surface is imposed at a distance from the wall where the velocity value is equal to the desired velocity shift $\Delta u^+(k_s^+)$. As a result, friction is increased.

With this purpose, a wall condition is imposed for each transported turbulent quantity at a distance $d_0$ from the smooth wall and not at the wall itself. However, for the $k-\omega-$SST model, the normal distance to the wall only appears at functions $F_1$ and $F_2$ [20]. This makes the required $d_0$ distance to be negligible. Consequently, Aupoix simplified the $d_0$ distance for $k-\omega-$SST corrections so that the modified wall condition for $k$ and $\omega$ could be set at the wall.

This strategy was applied by Aupoix to two different empirical sets, one aimed to match Nikuradse's experiments [11] and the other matches Colebrook's ones [25,26]. Equations (9)–(11) include the nondimensional formulation used for Nikuradse's empirical relationship. The reader is referred to Ref. [20] to see the formulation used for Colebrook's empirical relationship

$$k_w^+ = \max(0; k_0^+) \tag{9}$$

$$k_0^+ = \frac{1}{\sqrt{\beta^*}} \tanh\left[\left(\frac{\ln\frac{k_s^+}{30}}{\ln 8} + 0.5\left[1 - \tanh\frac{k_s^+}{100}\right]\right)\tanh\left(\frac{k_s^+}{75}\right)\right] \tag{10}$$

$$w_w^+ = \frac{400,000}{k_s^{+4}}\left(\tanh\frac{10,000}{3k_s^{+3}}\right)^{-1} + \frac{70}{k_s^+}\left[1 - \exp\left(-\frac{k_s^+}{300}\right)\right] \tag{11}$$

Both sets of BCs were used in several flat plate cases with and without APG. Finally, Aupoix recommended the use of Colebrook BC. It provides a better estimation of the $C_f$ tendency for high roughness. However, there is currently a lack of documentation about the use of these BCs in airfoil cases. Most of the literature applications to airfoil flows are focused on Wilcox's and Hellsten's corrections [21,30]. Hence, this study intends to contribute to the knowledge of Aupoix's BCs application on thick airfoils used in the wind energy industry.

## 3 Numerical Setup

The open-source CFD solver OPENFOAM v5.0 is used for the computations of this study. The flow is assumed to be incompressible and steady. The SIMPLEC algorithm is used to solve the N–S equations. A second-order linear upwind scheme is used for equations discretization. A residual value lower than $1 \times 10^{-6}$ is reached for every flow variable. For the flat plate case, a total number of 5000 iterations are required to reach convergence, whereas 30,000 iterations are required for airfoil cases. Additionally, a two-dimensional approach is followed using an empty boundary condition on sides normal to the spanwise direction.

Fully turbulent models are taken into account to model the roughness effect. The $k-\omega-$SST is the turbulence model selected, as in Secs. 4 and 5. For the thick airfoil case, the turbulence model selection is explained in Sec. 6. Additionally, the different $k-\omega$ models are also taken into account for flat plate cases to correctly assess the BC's efficiency. Clean reference cases in Sec. 6 are the only transitional flow computations determined by $\gamma - \mathrm{Re} - \theta$ model.

Inlet and outlet BCs are used for the flat plate case whereas a far-field BC is used for the airfoil case to switch between inlet and outlet BC depending on the velocity vector sense. For the inlet, the turbulence decay produced by the $k-\omega-$SST model is considered. This decay depends on $k_\infty$ and $\omega_\infty$ set at inlet cells. The method of Spalart et al. [31] is used to estimate the decay and reach the desired TI level at the airfoil leading-edge.

A Neuman BC is chosen for smooth and rough walls to establish the turbulent viscosity value at the wall.

The value of $k$ and $\omega$ at the wall will depend on the assumed surface state. For the smooth surface, a null value is set to $k$ and the recommended Menter's expression (see Eq. (12)) is used for $\omega$. The rough surface specification will depend on the chosen BC method (explained in Sec. 2)

$$\omega_w = 10 \cdot \frac{6\nu}{\beta_1(\Delta d)^2} \tag{12}$$

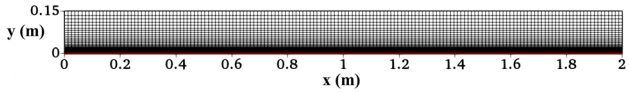


**Fig. 2 Structured mesh for flat plate cases**

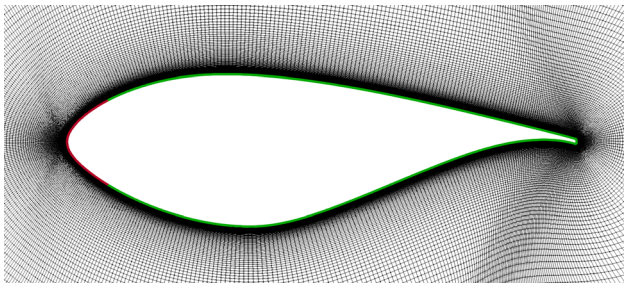

**Fig. 3 Structured O-grid for airfoil case of Sec. 6**

A near-wall model approach is adopted in this study, which means that no wall function is used between the wall and the first cell centroid above it. The mesh resolution is adjusted using the grid nodes placed along the normal direction to the wall. This is usually determined with a $y^+$ criterion. Menter [5] stated that $y^+$ should be lower than 1 for a correct use of $k$ and $\omega$ equations at the viscous sublayer region. On the other hand, studies on roughness modeling using $k-\omega-$SST, like the ones from Mendez et al. [21] and Langel et al. [13], concluded that $y^+$ should be below 0.5 under smooth conditions and below 0.1 under rough conditions. Hellsten and Laine [29] explained that the increment in velocity gradient at the rough wall makes the $y^+$ criterion more restrictive. Assuming a desired $y^+$ value of 0.1, a first cell height of $1.25 \times 10^{-6}$m is set for flat plate cases and $1.12 \times 10^{-6}$m for airfoil cases.

**3.1 Grid for Flat Plate Cases.** A mesh dependency study was carried out by Hellsten and Laine [29] to assess the needed resolution to correctly model the flow field. Their conclusions have been used in this study. A mesh resolution of $160 \times 96$ is finally used. A total number of 15,105 cells were determined. The structured mesh is shown in Fig. 2.

**3.2 Grid for Airfoil Cases.** An O-grid computational domain has been selected for every airfoil case. A radius $R$ of 40 times the airfoil chord length is used following Sorensen et al. [32] recommendations. The mesh around the airfoil is shown in Fig. 3.

The grid convergence index (GCI) method [33] was used to choose the mesh resolution. A fine mesh was first obtained following the recommendations provided in [32]. A constant $y^+$ of the first cell centroid above the wall was employed for each mesh and angle of attack (AoA). Three meshes were built from fine to coarse: L1 with 130,560 cells, L2 with 66,206 cells and L3 with 16,770 cells.

As Roache [33] indicates, if the ratio $GCI_{23}/r^p GCI_{12} \approx 1$, grid convergence can be assumed.

Most of the cases provided a suitable GCI ratio, as shown in Table 1. Besides, L1 mesh was modified to meet $y^+$ requirements of the roughness corrections and a finer mesh was obtained. A total number of 530 grid points were used to discretize the airfoil geometry while 270 grid points were used along the normal direction to the airfoil. This combination resulted in $1.4 \times 10^5$ cells.

**Table 1 Results for $\gamma-\mathrm{Re}-\theta$ turbulence model**

| Aero. coefficient | AoA (deg) | $GCI_{23}/r^p GCI_{12}$ |
|---|---|---|
| $C_L$ | –6 | 1.0007863 |
| | 12 | 1.009847 |
| $C_D$ | –6 | 0.976923 |
| | 12 | 0.912863 |

**Table 2 $k_s$ values derived from the ratios $k_s/L$ used by Hellsten and Laine [29] and using a flat plate length $L$ of 2 m**

| Case | $k_s/L$ | $k_s$ |
|---|---|---|
| 1 | 0.0001 | 0.0002 |
| 2 | 0.00025 | 0.0005 |
| 3 | 0.0005 | 0.001 |
| 4 | 0.001 | 0.002 |
| 5 | 0.0015 | 0.003 |

## 4 Flate Plate Case

Hellsten and Laine [29] used flat plate cases to demonstrate that his correction for $k-\omega-$SST works for different roughness regimes. Five cases were studied with the different $k_s$ values that are described in Table 2. A $k_s^+$ regime along the flat plate was obtained by each $k_s$ due to the variation in frictional velocity $u_\tau$ along the plate. A zero pressure gradient flat plate was used. Computational results were compared with empirical relationships, Nikuradse relationship for $\Delta u^+$ [11] and Mills–Hang relationship for $C_f$ development along the flat plate. As a result, SST limiter was disabled under different rough conditions.

Hellsten and Laine [29] set a maximum Reynolds number based on the stream-wise distance ($\mathrm{Re}_x$) of $5 \times 10^6$. In this study, the flat plate length is around 2 m after assuming a freestream velocity of 40 m/s and a kinematic air viscosity $\nu$ of $1.47 \times 10^{-5}$ m$^2$/s. The BL thickness $\delta$ is estimated using the empirical relationship given by Schlichting and Gersten [24]. The maximum $\delta$ is 0.04 m. Consequently, a total flat plate height of 0.15 m ensures the correct modeling of the defect layer and wake region of the BL.

Equivalent sand grain heights were scaled with the flat plate length ($L$) in Hellsten and Laine [29]. Table 2 summarizes the $k_s$ values used in this study.

**4.1 Flat Plate Results.** Hellsten and Laine [29] analyzed the roughness effect on $u^+$ for a certain stream-wise location. This location was scaled with the $k_s$ value as $x/k_s$. In this study, the location is computed to be at 1.085 m from the flat plate inlet.

This study starts with the comparison of the implementation of Hellsten's correction with the results presented in Hellsten and Laine [29]. Table 3 demonstrates the reliability of the comparison. The $y^+$ value of the first cell centroid above the wall is small enough to capture the viscous-sublayer. Besides, an increment in $y^+$ and $u_\tau$ is shown in rough cases compared with clean ones. This shows the relevance of taking into account roughness for the mesh generation. Rough BLs are made nondimensional using its corresponding $u_\tau$ value.

Hellsten and Laine [29] normalized the normal distance to the wall $y$ with the equivalent sand grain height $k_s$ to provide with unique comparison for every used $k_s$ value, as shown in Fig. 4. Although the $k_s^+$ values of this study are slightly higher than the ones provided in Hellsten and Laine [29], the same tendency is obtained between both CFD approaches. All lines approach the empirical relationship for low values of $y/k_s$. However, this effect is lost when $k_s$ is increased. The cases 4 and 5 present an

**Table 3 Values are computed with respect to the clean case ($y_0^+ = 0.069$ and $u_\tau = 1.55$)**

| Case | 1 | 2 | 3 | 4 | 5 |
|---|---|---|---|---|---|
| $\Delta y_0^+$ | 0.012 | 0.019 | 0.027 | 0.036 | 0.042 |
| $\Delta u_\tau$ | 0.27 | 0.44 | 0.61 | 0.81 | 0.95 |

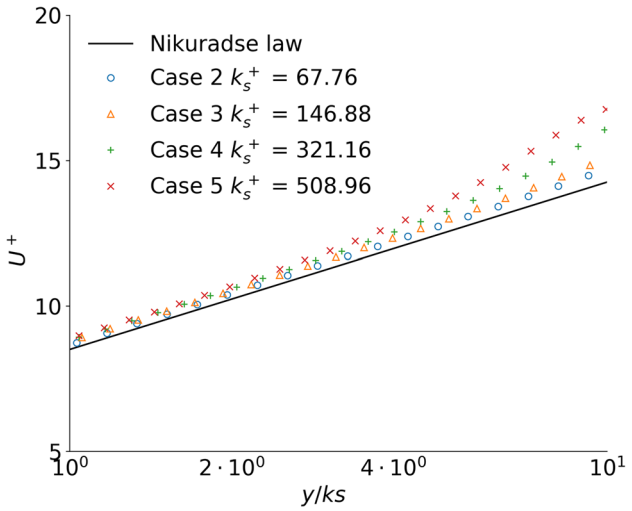


**Fig. 4 Scaling plot for different cases using Hellsten's correction. Nikuradse empirical relationship is represented in solid line.**

overestimation of $u^+$ compared with the cases 2 and 3, which was also obtained by Hellsten and Laine [29]. Aupoix [20] remarked this drawback of the Wilcox's BC along with Hellsten's correction for the fully rough regime, which is the regime reached by the cases 4 and 5. The similarity between Hellsten and Laine [29] and the presented results, verifies the Hellsten's correction implementation at the OPENFOAM code.

*4.1.1 Boundary Conditions Performance in Fully Rough Regime (Case 5).* Case 5 has been selected to compare the results provided by the studied combinations of BCs and the $k-\omega$ turbulence models. The reason for this selection is that $\Delta u^+$ underestimation was mainly reported by Aupoix for the fully rough regime ($k_s^+ > 70$).

Figure 5 shows that the Standard $k-\omega$ turbulence model along with the Wilcox's BC provides with correct estimations of $u^+$. Additionally, a correct implementation of the Wilcox's BC is verified. The BSL model is typically assumed to be the successor of the Standard $k-\omega$, since it removes the dependency on free-stream conditions provided by the Standard $k-\omega$. For the BSL turbulence model, the same $k_s^+$ as in the Standard $k-\omega$ model is obtained. Additionally, the BSL improves the modeling of the wake region because the equations of the $k-\epsilon$ model are enabled

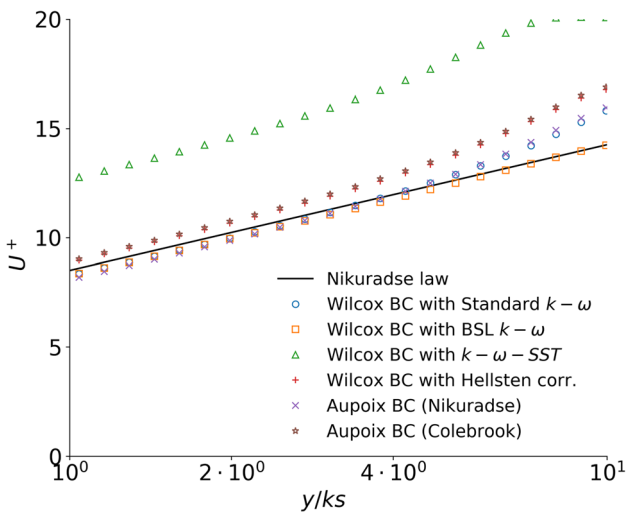


**Fig. 5 Scaling plot for Case 5 and different BCs. Nikuradse empirical relationship is represented in solid line.**

in that region. The results from the BSL model of this study are in good agreement with the one obtained by Hellsten and Laine [29].

The failure of the Wilcox's BC due to the presence of the SST limiter is clearly shown in Fig. 5 by the results labeled as Wilcox BC with $k-\omega-$SST. There is an underestimation of $k_s^+$, which is translated into an overestimation of the $u^+$ value. Aupoix [18] also stated this failure for different roughness regimes.

The Hellsten's correction solves the SST problem, but as shown in Fig. 5, it still deviates from Nikuradse's relationship. The result of the Aupoix BC based on Nikuradse's data is almost identical to the result from the BSL model. Consequently, this BC shares the SST advantages and it complies with Nikuradse's empirical relationship. On the other hand, the Aupoix's BC based on Colebrook data predicts a lower velocity shift than the Nikuradse one. This is justified by the difference between the empirical relationships. Even so, this last BC expression was highly recommended by Aupoix because it is more consistent with $\kappa$ constant used in $k-\omega-$SST and it provides better performance in fully rough regimes than other BCs.

## 5 Airfoil Cases From Literature

Two airfoil cases are taken from literature to support the confidence in the methodology followed in this study. These cases were used by Mendez et al. [21] to validate the use of the Hellsten's correction along with Wilcox's BC. A ratio $k_s/k_{tech} = 1$ was used by Mendez et al. [21], which is also assumed for every computation presented in this section.

The first case is based on a S809 airfoil that was tested in OSU wind tunnel [34] at a Re of $1 \times 10^6$. Grains were distributed on the airfoil leading-edge with a normalized height $k_{tech}/c$ of $1 \times 10^{-3}$. The BCs for roughness condition are applied to the first 11%c on both airfoil sides.

An over-prediction of $C_{Lmax}$ is provided for high values of $C_{Dp}$ by all BC used. This is justified by a RANS limitation [35]. A shift in lift slope from numerical solution to the experimental data is reported as observed by Mendez et al. [21]. A reduction of this overestimation is given by Aupoix BCs. Finally, the results show a good agreement between $C_L$ and $C_{Dp}$ values.

The second case is based on the NACA0012 airfoil. This airfoil was tested at the Two-Dimensional Low-Turbulence Pressure Tunnel at NASA Langley Research Center (Hampton, VA). The Reynolds number was 6 million. Carborundum grains were glued to the first 8%c on both airfoil sides following NACA standard method [36]. In this study, a $k_{tech}/c = 6 \times 10^{-4}$ is used.

The similarity among the three BCs shown for the S809 airfoil case, is also found for the NACA0012 symmetrical airfoil case. For low values of $C_D$, Fig. 6 shows a good agreement among all BC used. However, for high angles of attack, Aupoix BCs entail a more significant roughness effect than the one measured. In contrast, Wilcox's BC provides an over-prediction of $C_{Lmax}$. Similar

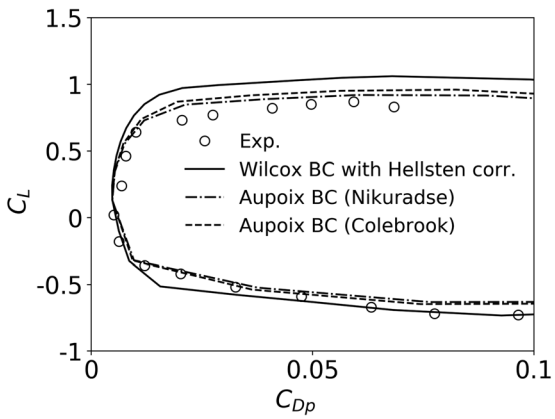


**Fig. 6 $C_L$ versus $C_{Dp}$ for S809 airfoil case**

experiments about distributed roughness on NACA0012 airfoil, as the one of Kerho and Bergg [12], revealed transitional flow over rough elements. Langel et al. [13] emphasized the importance of modeling transitional flow for those experiments. Even though it was done for a lower Reynolds number than six million, this could question the fully turbulent assumption adopted for this case (Fig. 7).

In summary, the implementation of the Wilcox's BC and Hellsten's correction shows a good agreement with the results of Mendez et al. [21]. For a moderate flow regime, defined by low Re and low $C_D$ values, the results from Aupoix BCs are in the order of the Wilcox's ones.

## 6 Application to Thick Airfoils With Industrial Relevance

All BCs are applied to a 30% thick airfoil. Thick airfoils are quite sensitive to roughness compared with thinner airfoils [37]. Consequently, this kind of airfoils can provide with a wide variety of flow regimes under rough conditions. Besides, there is structural advantage in using these airfoils for modern wind turbine blades [37]. The studied airfoil is property of Nordex Energy Spain S.A.U. Experiments from Gutiérrez et al. [10] are taken to validate the test case.

Gutiérrez et al. [10] tested this airfoil in the Low-Speed Low-Turbulence Wind Tunnel (LSL-LTT) of the Delft University of Technology. The airfoil model with a chord length of 0.6 m and a span length of 1.25 m was tested at a freestream velocity of 75 m/s with a turbulence level of 0.07% (corresponding to $\mathrm{Re} = 3 \times 10^6$). For more information about the tests, the reader is referred to [10].

Sandpaper was installed from the leading-edge to the first 8%c on both airfoil sides following NACA standard method [36]. A sandpaper with a grit number of 100 was selected. This grit number corresponds with a grain height ($k_g$) of 162 $\mu$m.

Transitional flow modeling over distributed roughness on airfoil leading-edges was studied by Langel et al. [13]. A subcritical range of the roughness Reynolds number ($Re_{ks}$) was defined between 100 and 400. Above this range, the flow is in a turbulent state. For this thick airfoil case, the maximum value of $Re_{ks}$ is estimated to be higher than 2000 at an AoA of 0 deg. This parameter is based on $k_s$ and the tangential velocity component at a $k_s$ distance above the wall. For $Re_{ks}$ estimation, an undisturbed BL is computed using $k-\omega-$SST. This assumption was also used by Langel et al. [13]. Additionally, infrared thermography images confirmed a turbulent state around the entire airfoil during the test. This justifies the use of $k-\omega-$SST as the turbulence model in the CFD modeling of this study.

In this study, conditions pertaining to an airfoil with mild separation have been chosen. This choice is motivated by RANS approach limitations when computing flow separation [35]. Apart from the expected flow separation on the airfoil suction side beyond $C_{Lmax}$, Gutiérrez et al. [10] measured considerable flow separation on the airfoil pressure side produced by roughness for low AoA. In this study, the analyzed AoA range corresponding to the condition mentioned above is defined from 4 to 9 deg.

**Table 4 Dimensionless heights due to sandpaper**

| $k_g/c$ | $k_d/c$ | $k_f/c$ | $k_{tech}/c$ |
|---|---|---|---|
| 0.00027 | 0.0000834 | 0.000834 | 0.00116 |

**6.1 Equivalent Sand Grain Value $k_s$ Used.** As it was remarked by Aupoix [18], the main drawback of the equivalent sand grain approach is its dependence on the used $k_s$ value. In an ideal situation, the $k_s$ value should be equal to the averaged grain height $k_g$ to ensure a ratio $k_s/k_{tech}$ approximated to 1. However, in practice, this was not achievable in the experiments of Gutiérrez et al. [10] because of the employment of the sandpaper with a finite support layer. As a result, an offset of $k_f$ from the airfoil surface is determined. Additionally, double-sided tape was used to attach the sandpaper to the airfoil leading-edge. This tape contributes to the offset with a thickness of $k_d$.

The $k_{tech}$ used in this study is the sum of $k_g$, $k_f$ and $k_d$ terms (see Table 4). The sum of $k_d$ and $k_f$ is the 78% of the offset which is considered a relevant amount.

Due to the difficulties in the derivation of $k_s$, a ratio $k_s/k_{tech}$ equal to 1 is chosen as an initial value. It is assumed that the sandpaper grain distribution is similar to the one used by Nikuradse [11]. This simplification is usually followed by other authors as [21,30]. As a next step, a $k_s$ fit is carried out to check possible improvements with respect to the initial value.

**6.2 Results for $k_s/k_{tech}=1$.** The velocity distribution in the logarithmic region of the BL and the $C_p$ on the airfoil surface are investigated to validate the correctness of the BCs to emulate the roughness effect.

In Figure 8, the $C_p$ results of all BCs are compared with pressure tabs measurements for an AoA of 5 deg. Wilcox's BC results in an underestimation of the roughness effects compared to Aupoix's BCs. A lower $C_p$ value is predicted by Wilcox's BC on the airfoil suction side while this difference is reduced on the airfoil pressure side. Aupoix's BCs provide with better $C_p$ estimation. The difference in the empirical Eqs. (4) and (5) explains that Nikuradse BC entails the most significant $C_p$ modification. The BL result from Colebrook BC is in better agreement with the

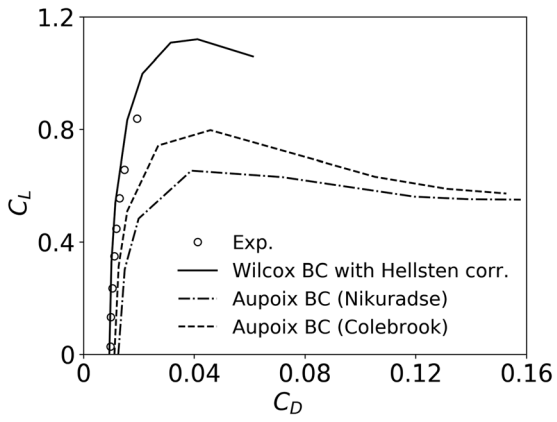


**Fig. 7 $C_L$ versus $C_D$ for NACA0012 airfoil case. Dots correspond to experimental data [36].**

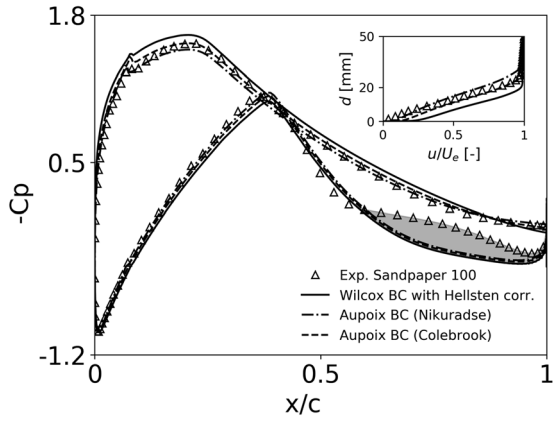


**Fig. 8 $C_p$ distribution for an AoA of 5 deg. PIV experimental boundary layer shown in small plot is extracted at $x/c = 0.87$ on the airfoil suction side.**

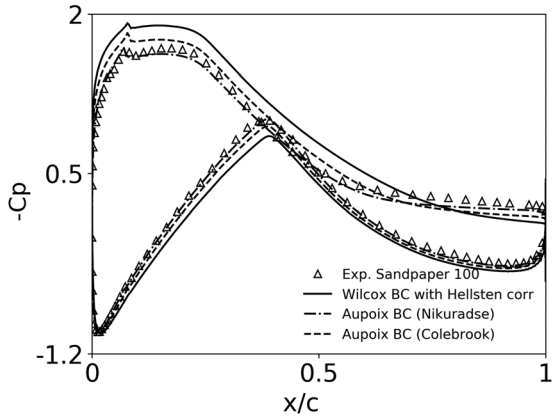


**Fig. 9 $C_p$ distribution for an AoA of 8 deg**

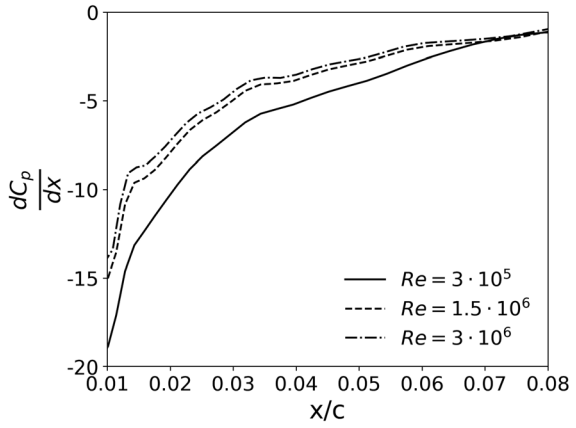


**Fig. 10 Pressure coefficient gradient on thick airfoil suction side for different Re**

measurements than Nikuradse BC, whereas a better performance is given by Nikuradse BC with respect to $C_p$ measurements.

Nevertheless, all BCs fail to predict $C_p$ at the gray region shown in Fig. 8. The $k_s$ parameter was varied to verify that this effect was not dependent on it. Although the analyzed AoA is inside the linear $C_L$ region of the rough polar, a small region of separated flow was still measured on the airfoil pressure side. This failure is related to RANS approach limitation to predict flow separation [35].

The underestimation produced by Wilcox's BC is more pronounced at relatively higher angles of attack, as demonstrated by Fig. 9. At an AoA of 8 deg, Nikuradse BC provides the most consistent result while the result from Colebrook BC is underestimated on the airfoil suction side. At this AoA, there is no separated flow on the airfoil pressure side and the CFD model is relatively more accurate in its prediction. RANS limitations are seen to be the cause of the failure shown in Fig. 8.

**6.3 Wilcox's Boundary Condition Limitation.** Due to the underestimation provided by Wilcox's BC in previous results, the $k_s$ parameter was increased to provide with more significant roughness effect than before. However, the resulting $C_p$ distribution was almost identical and no significant variation was detected for a wide range of the $k_s$ tested values. On the other hand, the Hellsten's function $F_3$ was checked to properly identify the roughness layer extension for each $k_s$ value. Consequently, the cause of the underestimation is related to Wilcox's boundary condition.

Comparing the results of Sec. 5 to the ones of Sec. 6, the S809 airfoil case determines better agreement in $C_p$ distribution than the thick airfoil case. Even though these computations were carried out using different Re, the geometry of thick airfoil leading-edges determine more pronounced pressure gradient than thin airfoils. Consequently, the boundary condition response against pressure gradient is crucial.

Both Aupoix and Wilcox BCs have been developed without taking into account the pressure gradient term in the momentum equation. As remarked by Aupoix [18], his strategy is only accurate for zero pressure gradient flows. Including the pressure gradient term in the momentum equation will introduce a numerical difference. However, this difference remains small compared to the influence of the wall friction term. This is corroborated with the agreement of the Aupoix's BCs in terms of pressure coefficient distributions shown in Figs. 8 and 9. On the other hand, there is no information about the sensitivity of the Wilcox's BC to pressure gradients. Even though all studied BCs are not adjusted to pressure gradient flows, the theory of the Aupoix's strategy seems to be relatively more suitable for these regimes. This theory acts on the BL profile itself whereas Wilcox's BC induces a different solution for the velocity profile by an arbitrary assignment of the $\omega$ value at the wall. As a result, Aupoix's BCs are more adapted to pressure gradient variations than Wilcox's BC due to the local effect over the velocity profile.

To investigate the BC adaptation to pressure gradients, the free-stream velocity is reduced for the same airfoil chord length obtaining a Reynolds number range from $3 \times 10^5$ to $3 \times 10^6$. Figure 10 shows a reduction of the $C_p$ gradient with the velocity increase. For all Reynolds numbers, a favorable pressure gradient is provided by the leading-edge geometry of the thick airfoil. On the other hand, Fig. 11 shows the similarity in $k^+_{smax}$ estimation depending on Reynolds number. For each computation, $k_s^+$ values are postprocessed following Eq. (3) and the maximum value is found. These maximum values were always found on the airfoil suction side because the AoA was always positive. For low Re, the favorable pressure gradient is higher, $k^+_{smax}$ is lower and the prediction is almost identical among the three BCs. However, once velocity is increased, the prediction among the three BCs diverges. Although the pressure gradient magnitude is reduced for high $Re$, it is combined with a higher value of $k_s^+$. This can magnify the difference in the eddy viscosity established by the BCs resulting in a different flow solution.

**6.4 Summary of Airfoil Performance Versus Boundary Condition.** The overall performance of the modeling can be verified with the airfoil aerodynamic coefficients. Figures 12 and 13 show, respectively, for clean and rough configurations the $C_L$ and $C_D$ polar curves. The $C_L$ in smooth conditions slightly deviates from wind tunnel measurements but the $C_D$ is in agreement with measurements. On the other hand, methods as $k - \omega -$ SST or

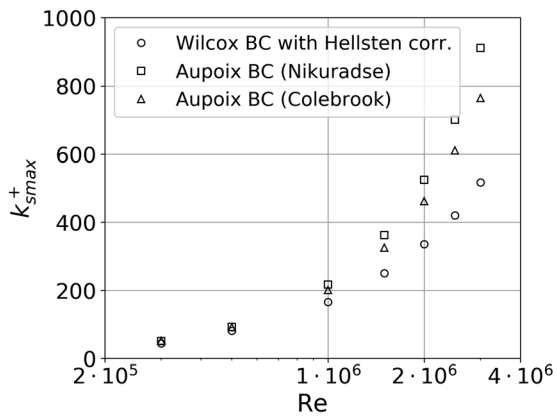


**Fig. 11 Development of maximum value of $k_s^+$ for different Re. Values are extracted on the rough leading-edge from the CFD result.**

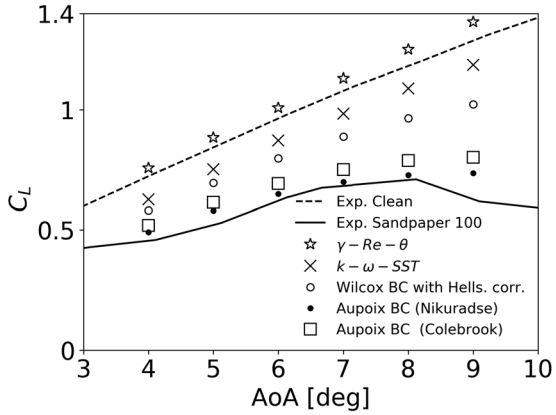


**Fig. 12 $C_L$ versus AoA for all models used in this study. Dash line indicates wind tunnel measurements assuming a smooth wall. Solid line is related to sandpaper attachment on the airfoil leading-edge.**

Wilcox's BC provide with underestimated effects of roughness. This comparison evidences that the use of $k - \omega - \text{SST}$ without any roughness correction is not appropriate for modeling roughness effects on airfoils. The only difference is that the BL is modeled in a turbulent state from the airfoil leading-edge neglecting the laminar BL emulation done by $\gamma - \text{Re} - \theta$ model. Finally, the previously explained Wilcox's BC limitation has significant consequences in the prediction of airfoil performance. The most significant impact is determined as an over-prediction of $C_L$.

Aupoix's BCs provide with better performance under pressure gradient for different $k_s^+$ values. Nikuradse BC provides a suitable $C_L$ prediction for 7 and 8 deg which is improved by Colebrook BC with the $k_s$ fit. For relatively lower angles of attack, the RANS limitations result in an overestimated $C_L$. With respect to $C_D$, Aupoix's BCs prediction is in agreement with measurements. Flow separation introduces coherent flow structures which determines difficulties in the measurement of a converged $C_D$. In order to reduce the uncertainty on the $C_D$ measurements, averaging between wake rake and pressure tabs results has been carried out. The computed tendency of $C_L$ is in agreement with the one measured whereas the tendency of $C_D$ is completely different as shown in Fig. 13.

Additionally, the BCs behavior is the same beyond $C_{Lmax}$, as demonstrated by the results at AoA of 9 deg.

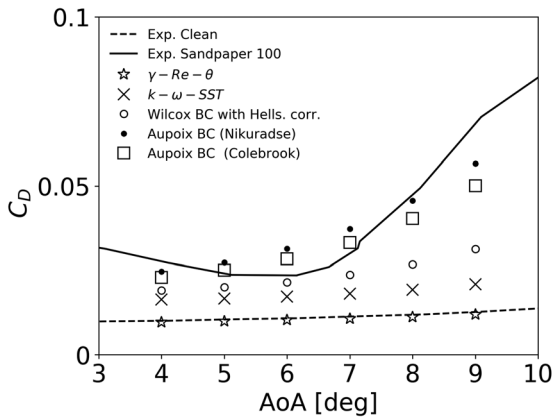


**Fig. 13 $C_D$ versus AoA for all models used in this study. Dash line indicates wind tunnel measurements assuming a smooth wall. Solid line is related to sandpaper attachment on the airfoil leading-edge.**

## 7 Conclusions

A study has been carried out to quantify the limits of the current roughness corrections for $k - \omega$ turbulence models once they are applied to airfoil computations under the equivalent sand grain approach. Wilcox's BC was chosen due to its extensive use in literature. To ensure the compatibility of this BC with the turbulence model, Hellsten's correction is used.

The correctness of the implementation of the BCs is first validated with flat plate cases found in the literature whose results are in agreement with the ones presented by Hellsten and Laine [29]. Additionally, Aupoix BCs is verified to be the same as in Aupoix [20]. The BC based on Colebrook's Eq. (5) is comparable with Wilcox's BC as indicated by Aupoix [20] and the result of the Nikuradse BC fulfills Nikuradse's Eq. (4).

The main limitation shown in this study is the sensitivity of the BCs to pressure gradients, as their formulation does not account for them. While the impact of this limitation was lower for the S809 and NACA0012 airfoils, it had a significant impact on the aerodynamic performance of the thick airfoil case. Wilcox's BC along with Hellsten's correction gives an underestimation of the airfoil $C_p$ distribution. This error is demonstrated to be directly proportional to the freestream velocity. In contrast, Aupoix's BCs are concluded to be more adaptable to pressure gradients under different $k_s^+$ values. However, further research should be done to understand Aupoix's BCs behavior for high Re near $C_{Lmax}$.

Reynolds-averaged Navier–Stokes limitations for detached flows are a current problem for roughness modeling in thick airfoils as an overestimation of $C_L$ and a wrong tendency of $C_D$ is determined. This limitation is concluded not to be related to the BCs because it is not dependent on the $k_s$ value and it is reported for every BC.

## Acknowledgment

The authors of this study would like to acknowledge Antti Hellsten for the help given in the understanding and implementation of the $F_3$ function.

## Nomenclature

$c$ = airfoil chord length (m)
$k$ = turbulent kinetic energy ($m^2/s^2$)
$p$ = order of convergence of Richardson extrapolation
$r$ = rate of convergence of Richardson extrapolation
$u$ = tangential velocity component to wall surface (m/s)
$y$ = normal distance to the wall (m)
$L$ = flat plate length (m)
$R$ = O-grid radius (m)
$|\mathbf{S}|$ = scalar measure of the strain-rate tensor ($s^{-1}$)
$a_1$ = Bradshaw's structural parameter
$b_1$ = SST limiter parameter
$d_0$ = wall shift for roughness correction
$k_d$ = double-sided tape thickness (m)
$k_f$ = sandpaper fabric thickness (m)
$k_g$ = averaged sandpaper grain height (m)
$k_s$ = equivalent sand grain height (m)
$k_{tech}$ = technical roughness height (m)
$k_w$ = turbulent kinetic energy at the wall ($m^2/s^2$)
$k_\infty$ = free stream turbulent kinetic energy ($m^2/s^2$)
$u_\tau$ = friction velocity (m/s)
$C_L$ = lift coefficient
$C_D$ = drag coefficient
$C_{Dp}$ = pressure drag coefficient
$C_f$ = friction coefficient
$C_p$ = pressure coefficient
$F_1, F_2$ = blending functions of $k - \omega - \text{SST}$
$F_3$ = Hellsten's correction
$S_R$ = factor defined in Wilcox's BC to modify $\omega$
$u^+$ = nondimensional tangential velocity component to wall surface
$y^+$ = nondimensional normal distance to the wall

$C^+$ = logarithmic law constant
$k_s^+$ = nondimensional equivalent sand grain height
$k_w^+$ = nondimensional turbulent kinetic energy at the wall
Re = Reynolds number based on c
TI = turbulence intensity
$GCI_{12}$ = grid convergence index for meshes L1 and L2
$GCI_{23}$ = grid convergence index for meshes L2 and L3
$B(k_s^+)$ = Nikuradse constant dependent on $k_s^+$
$\beta^*$,$\beta 1$ = turbulence model coefficients
$\Delta u^+$ = difference in $u+$ between smooth and rough solutions
$\kappa$ = von Karman constant
$\mu_t$ = eddy viscosity (kg/m s)
$\nu$ = kinematic air viscosity ($m^2/s$)
$\nu_t$ = kinematic eddy viscosity ($m^2/s$)
$\sigma_k$ = diffusion coefficient
$\omega$ = specific turbulence dissipation rate ($s^{-1}$)
$\omega_w$ = value of $\omega$ at the wall ($s^{-1}$)
$\omega_\infty$ = freestream $\omega$ value ($s^{-1}$)
$\omega_w^+$ = nondimensional $\omega$ value at the wall ($s^{-1}$)
$|\mathbf{S}|$ = scalar measure of the strain-rate tensor ($s^{-1}$)

## References


[1] Anderson, J., 2010, *Fundamentals of Aerodynamics*, The McGraw-Hill Companies, Inc., New York, pp. 1025–1026.
[2] Tabib, M., Rasheed, A., Siddiqui, M. S., and Kvamsdal, T., 2017, "A Full-Scale 3D Vs 2.5D Vs 2D Analysis of Flow Pattern and Forces for an Industrial-Scale 5 MW NREL Reference Wind-Turbine," Energy Procedia, **137**, pp. 477–486.
[3] Wilcox, D. C., 2006, *Turbulence Modelling for CFD*, 3rd ed., D C W Industries, Canada, CA, pp. 182–185.
[4] Spalart, P. R., and Allmaras, S. R., 1994, "One-Equation Turbulence Model for Aerodynamic Flows," Recherche Aerospatiale, AIAA Meeting Paper 30th Aerospace Sciences Meeting and Exhibit, Reno, NV.
[5] Menter, F., 1993, "Zonal Two Equation k–w Models Turbulence for Aerodynamic Flows," AIAA Meeting Paper, 23rd Fluid Dynamics, Plasmadynamics and Lasers Conference, Orlando, FL.
[6] Langtry, R. B., 2006, "A Correlation-Based Transition Model Using Local Variables for Unstructured Parallelized CFD Codes," Ph.D. thesis, University of Stuttgart, Stuttgart, Germany.
[7] Walters, D. K., and Cokljat, D., 2008, "A Three-Equation Eddy-Viscosity Model for Reynolds-Averaged Navier–Stokes Simulations of Transitional Flow," J. Fluids Eng., Trans. ASME, **130**(12), p. 121401.
[8] Bak, C., Forsting, A. M., and Sorensen, N. N., 2020, "The Influence of Leading Edge Roughness, Rotor Control and Wind Climate on the Loss in Energy Production," J. Phys. Conf. Ser., **1618**, p. 052050
[9] Ehrmann, R. S., and Submitted, 2014, "Effect of Surface Roughness on Wind Turbine Performance," Ph.D. thesis, Texas A&M University, College Station, TX.
[10] Gutiérrez, R., Llórente, E., Echeverría, F., and Ragni, D., 2020, "Wind Tunnel Tests for Vortex Generators Mitigating Leading-Edge Roughness on a 30% Thick Airfoil," J. Phys.: Conf. Ser., **1618**, p. 052058.
[11] Nikuradse, J., 1936, "Laws of Flow in Rough Pipes," National Advisory Committee for Aeronautics, Washington, Technical Report No. 4.
[12] Kerho, M. F., and Bergg, M. B., 1995, "Effect of Large Distributed Leading-Edge Roughness on Boundary Layer Development and Transition," 13th Applied Aerodynamics Conference, San Diego, CA, pp. 322–334.
[13] Langel, C. M., Chow, R., Dam, C. P. V., and Maniaci, D. C., 2017, "RANS Based Methodology for Predicting the Influence of Leading Edge Erosion on Airfoil Performance," Technical Report, Sandia Laboratories, Albuquerque, NM, pp. 1–170.
[14] Drela, M., 1989, "Xfoil: An Analysis and Design System for Low Reynolds Number Airfoils," Low Reynolds Number Aerodynamics. Proceedings of the Conference, Notre Dame, IN.
[15] Van Rooij, R., 1996, "Modification of the Boundary Layer Calculation in Rfoil for Improved Airfoil Stall Prediction," The Netherlands, DUWIND Report IW-96087R.
[16] van Ingen, J., The eN Method for Transition Prediction. Historical Review of Work at TU Delft, AIAA Meeting Paper, 38th AIAA Fluid Dynamics Conference and Exhibit, Seattle, Washington, DC, June 23–26, pp. 1–49.
[17] Kruse, E., Sørensen, N., Bak, C., and Nielsen, M., 2020, "CFD Simulations and Evaluation of Applicability of a Wall Roughness Model Applied on a NACA 633–418 Airfoil," Wind Energy, **23**(11), pp. 2056–2067.
[18] Aupoix, B., 2007, "A General Strategy to Extend Turbulence Models to Rough Surfaces: Application to Smith's k–L Model," J. Fluids Eng., Trans. ASME, **129**(10), pp. 1245–1254.
[19] Ribeiro, A., Casalino, D., Fares, E., and Choudhari, M., 2016, "Direct Numerical Simulation of an Airfoil With Sand Grain Roughness on the Leading Edge," NASA Technical Memorandum 219363 (October 2016).
[20] Aupoix, B., 2015, "Roughness Corrections for the k-$\omega$ Shear Stress Transport Model: Status and Proposals," ASME J. Fluids Eng., **137**(2), p. 021202.
[21] Mendez, B., Muñoz, A., and Munduate, X., 2015, "Study of Distributed Roughness Effect Over Wind Turbine Airfoils Performance Using CFD," 33rd Wind Energy Symposium, Kissimmee, FL, Jan. 5–9, pp. 1–20.
[22] Bangga, G., Kusumadewi, T., Hutomo, G., Sabila, A., Syawitri, T., Setiadi, H., Faisal, M., Wiranegara, R., Hendranata, Y., Lastomo, D., Putra, L., and Kristiadi, S., 2018, "Improving a Two-Equation Eddy-Viscosity Turbulence Model to Predict the Aerodynamic Performance of Thick Wind Turbine Airfoils," J. Phys. Conf. Ser., **974**, p. 012019.
[23] Jasak, H., Jemcov, A., and Tukovic, Z., 2007, "OpenFOAM: A C ++ Library for Complex Physics Simulations," International Workshop on Coupled Methods Numerical Dynamics, Dubrovnik, Croatia.
[24] Schlichting, H., and Gersten, K., 2016, "Boundary-Layer Theory," 8th Revised and Enlarged Edition, Springer-Verlag Berlin Heidelberg, Germany, pp. 529–534.
[25] Colebrook, C. F., White, C. M., and Taylor, G. I., 1937, "Experiments With Fluid Friction in Roughened Pipes," Proc. R. Soc. London. Ser. A – Math. Phys. Sci., **161**(906), pp. 367–381.
[26] Colebrook, C. F., 1939, "Turbulent Flow in Pipes, With Particular Reference to the Transition Region Between the Smooth and Rough Pipe Laws," J. Inst. Civ. Eng., **21**, pp. 113–156.
[27] Grigson, C., 1992, "Drag Losses of New Ships Caused by Hull Finish," J. Ship Res., **36**(02), pp. 182–196.
[28] Saffman, P. G., and Whitham, G. B., 1970, "A Model for Inhomogeneous Turbulent Flow," Proc. R. Soc. London. A. Math. Phys. Sci., **317**(1530), pp. 417–433.
[29] Hellsten, A., and Laine, S., 1997, "Extension of the k–$\omega$–SST Turbulence Model for Flows Over Rough Surfaces," 22nd Atmospheric Flight Mechanics Conference, New Orleans, LA, pp. 252–260.
[30] Ferrer, E., and Munduate, X., 2009, "CFD Predictions of Transition and Distributed Roughness Over a Wind Turbine Airfoil," 47th AIAA Aerospace Sciences Meeting Including the New Horizons Forum and Aerospace Exposition, Orlando, FL, pp. 1–16.
[31] Spalart, P. R., and Rumsey, C. L., 2007, "Effective Inflow Conditions for Turbulence Models in Aerodynamic Calculations," AIAA J., **45**(10), pp. 2544–2553.
[32] Sorensen, N. N., Mendez, B., Munoz, A., Sieros, G., Jost, E., Lutz, T., Papadakis, G., Voutsinas, S., Barakos, G. N., Colonia, S., Baldacchino, D., Baptista, C., and Ferreira, C., 2016, "CFD Code Comparison for 2D Airfoil Flows," J. Phys. Conf. Ser., **753**, p. 0820198.
[33] Roache, P. J., 1997, "Quantification of Uncertainty in Computational Fluid Dynamics," Annu. Rev. Fluid Mech., **29**(1), pp. 123–160.
[34] Ramsay, R. F., Hoffman, M. J., and Gregorek, G. M., 1995, "Effects of Grit Roughness and Pitch Oscillations on the S809 Airfoil," National Renewable Energy Lab. (NREL), Golden, CO, Technical Report No. NREL/TP-442-7817.
[35] Zhong, W., Tang, H., Wang, T., and Zhu, C., 2018, "Accurate RANS Simulation Ofwind Turbine Stall by Turbulence Coefficient Calibration," Appl. Sci., **8**(9), p. 1444.
[36] Abbott, I. H., and Von Doenhoff, A. E., 1959, "Theory of Wing Sections: Including a Summary of Airfoil Data," Dover Publications, Mineola, NY.
[37] Van Rooij, R. P. J. O. M., and Timmer, W. A., 2003, "Roughness Sensitivity Considerations for Thick Rotor Blade Airfoils," J. Sol. Energy Eng., Trans. ASME, **125**(4), pp. 468–478.